The Thermal Dehydrofluorination of GaPO-34 Revealed by NMR Crystallography

Daniel M. Dawson,[1*] Laurie E. Macfarlane,[1] Mahrez Amri,[2] Richard I. Walton[2] and Sharon E. Ashbrook[1*]

1. School of Chemistry, EaStCHEM and St Andrews Centre for Magnetic Resonance, University of St Andrews, North Haugh, St Andrews KY16 9ST, UK

2. Department of Chemistry, University of Warwick, Coventry, CV4 7AL, UK

ABSTRACT: Using a combination of solid-state NMR spectroscopy, powder X-ray diffraction (pXRD), thermogravimetry and periodic density functional theory (DFT) calculations, we investigate the calcination of the chabazite-type gallophosphate, GaPO-34 prepared with either 1-methylimidazole (mim) or pyridine (py) as the structure-directing agent (SDA) and fluoride as the charge-balancing anion. We demonstrate that, prior to SDA combustion, there is an unusual low-temperature dehydrofluorination step at ~330 °C for the mim material, but not for the py form. The DFT-derived structure for the dehydrofluorinated intermediate contains pentacoordinate Ga species with Ga–N bonds of 2.04 Å to the mim nitrogen atom, in addition to four Ga–O bonds to neighboring PO_4 tetrahedra. This observation is consistent with ^{71}Ga NMR spectroscopy, which shows that one third of the Ga is pentacoordinate with a large quadrupolar coupling constant of ~11 MHz. Powder X-ray diffraction measured *in situ* on heating shows the transient appearance of a distinct crystalline phase between 325 and 425 °C before the characteristic chabazite structure is seen, which is consistent with deydrofluorination prior to loss of the organic SDA. No such dehydrofluorinated intermediate structure is observed for the py form of GaPO-34, which is ascribed to the lower pK_a of pyridinium relative to 1-methylimidazolium.

Introduction

The many applications of zeolitic frameworks are well known and often arise from the highly specific interactions of "guest" species with the walls of the molecule-sized channels and pores of the framework.[1] The original zeolites were aluminosilicates, but many other families of zeolite-like materials (or "zeotypes") have since been developed. While the aluminophosphates (AlPOs)[2] are relatively well studied and have been modified by substitution of iso- and aliovalent cations (Mg^{2+}, Si^{4+}, *etc.*) to introduce catalytic behaviour (*e.g.*, Brønsted or Lewis acidity and redox activity), the closely related gallophosphates (GaPOs) have attracted less intense research interest. The synthesis of GaPOs is generally carried out in the presence of a cationic organic structure-directing agent (SDA) and a mineraliser (*e.g.*, F^- or HO^-). The SDA and mineraliser are incorporated into the structure of the "as-made" GaPO, typically with the anions bound to Ga to give some five- or six-coordinate sites in addition to the expected tetrahedral Ga, yielding an overall negatively charged framework. Charge neutrality is maintained by the SDA, which is located within the pores of the material. Calcination can remove the SDA/mineraliser ion pair, leaving the neutral, microporous $GaPO_4$ framework, which is composed of corner-sharing GaO_4 and PO_4 tetrahedra, in strict alternation. However, many calcined GaPOs are unstable, particularly to heating in the presence of water, meaning that the preparation of the microporous gallophosphate framework may be challenging.[3,4]

Calcined GaPO-34 (chabazite-type framework) is known to be stable in dry conditions,[3,4] although it is hygroscopic and unstable to a combination of heat and moisture.[5] As part of a wider investigation into gallium oxides and phosphates, we recently characterised several phases of GaPO-34, including the as-made, calcined and calcined-rehydrated forms[5] and noted the presence of an intermediate phase during the calcination of GaPO-34 containing 1-methylimidazolium fluoride (mimHF), but not when pyridinium fluoride (pyHF) was present. This intermediate phase was first noted by Schott-Darie *et al.*,[4] although only its powder X-ray diffraction (pXRD) pattern was reported, and no detail of its composition or structure was proposed.

In recent years, interest has grown in the use of strategies such as NMR crystallography and "SMARTER" crystallography, which combine information from NMR spectroscopy (and often first-principles calculations) with X-ray (or neutron) crystallography to provide an in-depth picture of both the local and long-range structure of a material, where these techniques could not individually have provided such information.[6-11] These approaches have been especially successful for microporous materials,[7,12-24] particularly with recent advances in both computational power and the accuracy and efficiency of calculations available.[25-27] In particular, we recently reported the application of this approach to GaPO-34A, a material that can be prepared from the same starting gel as GaPO-34, but which contains multiple levels of compositional, orientational and dynamic disorder that could not have been revealed or understood using a single characterisation

technique.[24]

In this work, we combine solid-state NMR spectroscopy, thermogravimetry, *in-situ* variable-temperature pXRD and density functional theory (DFT) calculations to investigate the calcination of GaPO-34 containing mimHF and pyHF within the pores. We show that, for GaPO-34[pyHF] (where the square brackets denote the extraframework species present), calcination occurs as a single step, whereas, for GaPO-34[mimHF], the calcination is a two-stage process, involving first dehydrofluorination to GaPO-34[mim], followed by loss of neutral 1-methylimidazole (mim). Such a two-stage calcination with low-temperature dehydrofluorination was unexpected and appears rare in phosphate zeotypes. While two previous studies have investigated the loss of HF on heating AlPOs, this was reported in both cases to be accompanied by loss of the organic species (*i.e.*, partial calcination rather than selective dehydrofluorination).[28,29] In the case of GaPO-34[mimHF], we demonstrate the controlled release of HF with retention of the neutral SDA, which may allow the material to act as a clean solid source of HF at moderate temperatures. The neutral mim remains in the pores to form a Ga···N Lewis acid-base adduct, leading to an unusual type of pentacoordinate Ga species.

Experimental Methods

GaPO-34[pyHF] and GaPO-34[mimHF] were prepared as previously reported.[5] Poorly crystalline ε-Ga_2O_3 was prepared by decomposition of hydrated gallium nitrate in air at 250 °C for 24 h. 0.5 g of this material was combined with 85 wt% aqueous H_3PO_4, 40 wt% aqueous HF and the SDA to give a gel of composition $Ga_2O_3 : P_2O_5 : HF : 70 H_2O : 1.7$ SDA. The gel was stirred at room temperature for 2 h, sealed in a Teflon autoclave liner and heated at 170 °C for 24 h. After cooling, the GaPO product was isolated by filtration and washed with H_2O. Note that the gel aging time is crucial, with GaPO-34 only forming with longer aging times, with GaPO-34A formed at shorter times.[30]

GaPO-34[mim] was prepared by heating GaPO-34[mimHF] to ~330 °C under air for 2 h. The sample was packed into a sealed vial while hot (~200 °C) and then packed (under air) into an NMR rotor immediately before the first NMR spectra were recorded. All NMR spectra shown for GaPO-34[mim], with the exception of the [71]Ga spectrum recorded at 20.0 T were obtained within 24 h to minimize uptake of ambient water.

A Bruker D8 diffractometer operating with Cu K$_{\alpha 1/2}$ radiation was used for variable-temperature pXRD experiments. The samples were packed into a ceramic holder and data measured in θ-θ geometry using a VÅNTEC solid-state detector, which permitted a typical diffraction pattern to be accumulated in around 3 min. The diffractometer was equipped with an Anton Parr XRK 900 reactor chamber, which allowed the sample to be heated above room temperature under flowing air. Before each data collection the temperature was allowed to equilibrate for 5 min.

A Mettler-Toledo TGA/DSC 1 Thermogravimetric Analyser was used to measure TGA and differential scanning calorimetry (DSC) simultaneously. Approximately 10 mg of powdered sample was placed in an aluminum pan and its mass monitored in static air upon heating to 1000 °C at a rate of 10 °C min^{-1}.

With the exception of [71]Ga, the solid-state NMR spectra were recorded using a Bruker Avance III spectrometer equipped with a 14.1 T wide-bore superconducting magnet. ^{1}H and ^{19}F NMR spectra were recorded with the samples packed into 1.3 mm zirconia rotors and rotated with a magic angle spinning (MAS) rate of 55 kHz. [1]H spectra were recorded with a rotor-synchronized DEPTH pulse sequence[31] to eliminate the probe background. Signal averaging was carried out for 64 (GaPO-34[mimHF]) or 256 (GaPO-34[mim]) transients with a recycle interval of 3 s. [19]F spectra were recorded with a rotor-synchronized spin-echo sequence. Signal averaging was carried out for 64 (GaPO-34[mimHF]) or 128 (GaPO-34[mim]) transients with a recycle interval of 3 s (GaPO-34[mimHF]) or 10 s (GaPO-34[mim]). ^{31}P and ^{13}C NMR spectra were recorded with the samples packed into 2.5 mm zirconia rotors and rotated at the magic angle at a rate of 25 (^{31}P) or 12.5 (^{13}C) kHz. [31]P spectra were recorded with signal averaging for 8 (GaPO-34[mim] and calcined GaPO-34) or 16 (GaPO-34[mimHF]) transients with a recycle interval of 300 s (GaPO-34[mimHF] and GaPO-34[mim]) or 3 s (calcined GaPO-34). [13]C spectra were recorded with cross polarization (CP) from ^{1}H, using a spin lock (ramped for ^{1}H) duration of 1 ms. Signal averaging was carried out for 2048 (GaPO-34[mimHF]) or 1024 (GaPO-34[mim]) transients with a recycle interval of 3 s. Two-pulse phase modulation (TPPM) decoupling of [1]H ($\nu_1 \approx 80$ kHz) was applied during acquisition.

[71]Ga solid-state NMR spectra were recorded using a Bruker Avance III spectrometer equipped with a 20.0 T wide-bore superconducting magnet at the UK 850 MHz Solid-State NMR Facility. The samples were packed into 1.3 mm rotors and rotated at a MAS rate of 60 kHz. The spectra were recorded using a rotor-synchronized spin-echo sequence with pulses of inherent flip angles of *ca.* 30° and 60°. Signal averaging was carried out for 4096 transients with a recycle interval of 0.5 s.

For all NMR spectra, chemical shifts are reported in ppm relative to $(CH_3)_4Si$ (^{1}H and ^{13}C), $CFCl_3$ (^{19}F), 85% aqueous H_3PO_4 (^{31}P) and 0.1 M aqueous $Ga(NO_3)_3$ ([71]Ga) using L-alanine (δ(NH_3) = 8.5 ppm, δ(CH_3) = 20.5 ppm), PTFE (δ = –122.7 ppm), BPO_4 ([31]P δ = –29.6 ppm) and $GaPO_4$ berlinite ([71]Ga δ$_{iso}$ = 111.1 ppm) as secondary solid references.

To generate an initial structural model for GaPO-34[mim], the optimized structure of as-made GaPO-34 was taken from Ref. 5, the NH protons, fluoride and water were removed and the 1-methylimidazole molecules were manually moved closer to the formerly fluorinated Ga species to facilitate more rapid optimization, as discussed below. This structure was optimized using the CASTEP density functional theory (DFT) code (version 19.11),[32] employing the GIPAW algorithm,[33] to reconstruct the all-electron wavefunction in the presence of a magnetic field for the calculation of NMR parameters. Calculations used the GGA PBE functional, with core-valence interactions described by ultrasoft pseudopotentials,[34] which were generated on the fly, accounting for scalar relativistic effects using ZORA.[35] A modified pseudopotential was used for Ga, as described by Cook *et al.*[36] A planewave cut-off energy of 60 Ry was used, and integrals over the Brillouin zone were performed using a Monkhurst-Pack grid with a k-point spacing of 0.04 2π Å^{-1}. Dispersion interactions were introduced using the scheme of Tkatchenko and Scheffler,[37] as implemented by McNellis *et al.*[38] Calculations were performed on a computing cluster at the University of St Andrews, consisting of 90 32-core Intel Broadwell nodes, Infiniband FDR interconnects, and a 300 TB GPFS distributed file system.

Calculations generate the shielding tensor in the crystal frame, σ, from which the calculated isotropic shielding is given

by $\sigma_{iso} = (1/3) \, \mathrm{Tr}\{\boldsymbol{\sigma}\}$, and the isotropic chemical shift by $\delta_{iso} = -(\sigma_{iso} - \sigma_{ref})/m$, where σ_{ref} is a reference shielding and m is a scaling factor. In this work, m = 1 for all nuclei and values of σ_{ref} of 171.0, 290.3 and 1741.0 ppm were used for ^{13}C, ^{31}P and [71]Ga, respectively, using as-made (dehydrated) GaPO-34 as the reference compound for ^{13}C and calcined dehydrated GaPO-34 as the reference compound for ^{31}P and [71]Ga).[39] The quadrupolar coupling constant ($C_Q = eQV_{ZZ}/h$) and the asymmetry parameter ($\eta_Q = (V_{XX} - V_{YY})/V_{ZZ}$) are obtained directly from the principal components of the electric field gradient tensor, **V**. Q is the nuclear quadrupole moment, for which a value 107 mb was used for [71]Ga.[40]

Results and Discussion

The calcination of GaPO-34[mimHF] and GaPO-34[pyHF] was followed by TGA/DSC, as shown in Figures 1(a and b). Both materials lose H_2O between 80 and 100 °C (~1.7% mass loss, corresponding to ~0.6 H_2O per formula unit, consistent with the crystal structure of GaPO-34[mimHF][4]). The calcination of GaPO-34[pyHF] then occurs in a single endothermic step (Figure 1b) between ~350 and 400 °C, consistent with the loss of pyHF. While the mass loss associated with calcination of GaPO-34[mimHF] begins at a similar temperature, calcination occurs in two endothermic steps and is not complete until ~500 °C, with the overall mass loss consistent with mimHF. The intermediate step in mass loss observed at ~400 °C is consistent with the loss of HF – see Supporting Information for further details. We therefore term this intermediate phase GaPO-34[mim], to denote the possible loss of HF from the parent GaPO-34[mimHF]. The presence of this intermediate is also clear in the *in-situ* variable-temperature pXRD patterns, shown in Figure 1(c), where a distinct crystallographic phase is apparent between 325 and 425 °C, which does not correspond to either the as-prepared GaPO-34[mimHF] or the calcined GaPO-34. While the temperature ranges in which this phase appears to exist are different when obtained by TGA/DSC and *in-situ* XRD, this discrepancy can be explained by the different heating rates and sample volumes used in the different measurements. Schott-Darie *et al.* also reported the isolation of an unidentified phase, obtained at 315 °C during the calcination of GaPO-34[mimHF], but assigned this observation merely to a "phase transition" without offering any further explanation.[4] The pXRD pattern of this phase was reported, and agrees well with the *in-situ* pXRD patterns assigned to GaPO-34[mim] in Figure 1(c), despite the discrepancy between the reported temperature at which this unidentified phase occurs. We attempted to obtain a higher-quality pXRD pattern of GaPO-34[mim] by pausing the heating once the *in situ* pXRD measurements indicated the phase change had occurred and then recording the pattern for a longer period of time. However, the resolution of the diffraction data obtained by this approach was still insufficient to allow indexing of the unit cell.
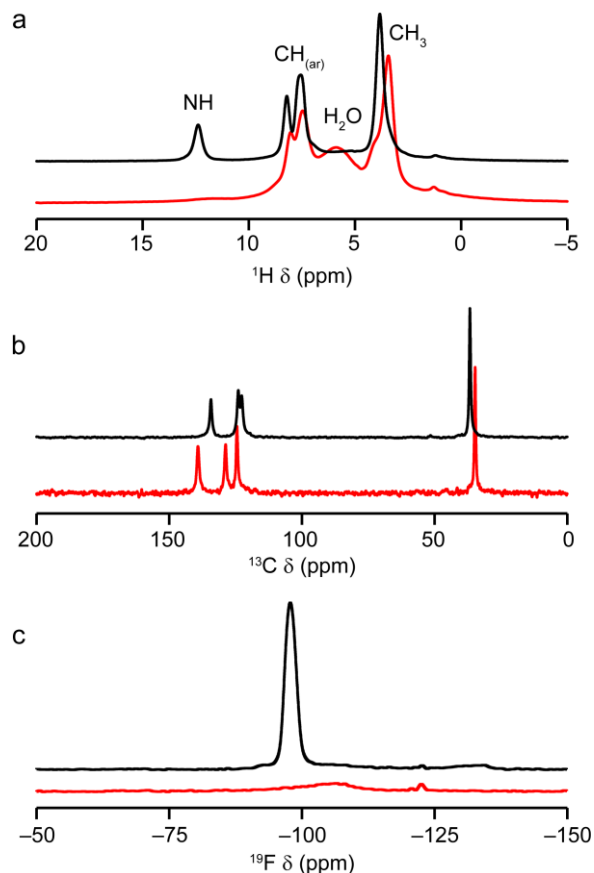
The ^{1}H NMR spectra of GaPO-34[mimHF] and GaPO-34[mim] are shown in Figure 2(a), and it can immediately be seen that the resonance at 12.4 ppm, previously assigned to N**H** in GaPO-34[mimHF][5] is absent in GaPO-34[mim], while the other resonances from the SDA are still present. The broad resonance at 5.9 ppm is attributed to H_2O within a portion of the sample that has been fully calcined (see below). It can also be noted that the relatively narrow resonances from the SDA are indicative of an ordered material (or possibly that the SDA is

dynamic). The ^{13}C NMR spectra of GaPO-34[mimHF] and
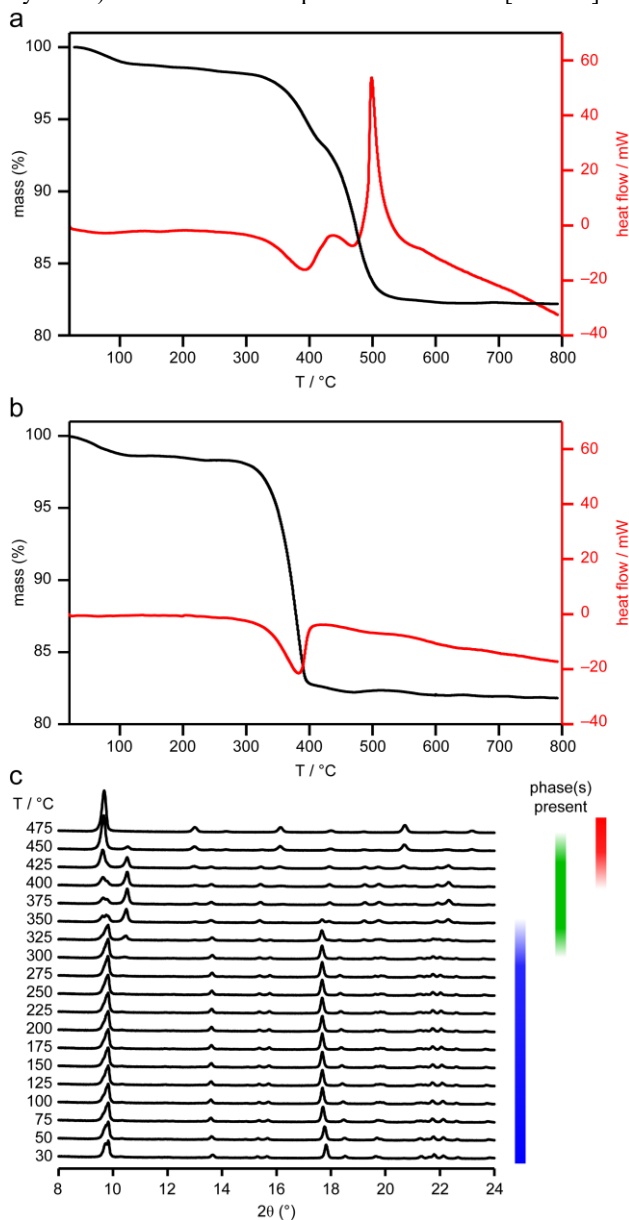
Figure 1. TGA (black, left axis) and DSC (red, right axis) traces for (a) GaPO-34[mimHF] and (b) GaPO-34[pyHF]. (c) *In-situ* pXRD patterns for GaPO-34[mimHF] heated from room temperature to 475 °C.[5] The colored bars indicate schematically which phase(s) are present at each temperature (blue = GaPO-34[mimHF], green = GaPO-34[mim] and red = calcined GaPO-34), highlighting the narrow window for preparing phase-pure GaPO-34[mim].
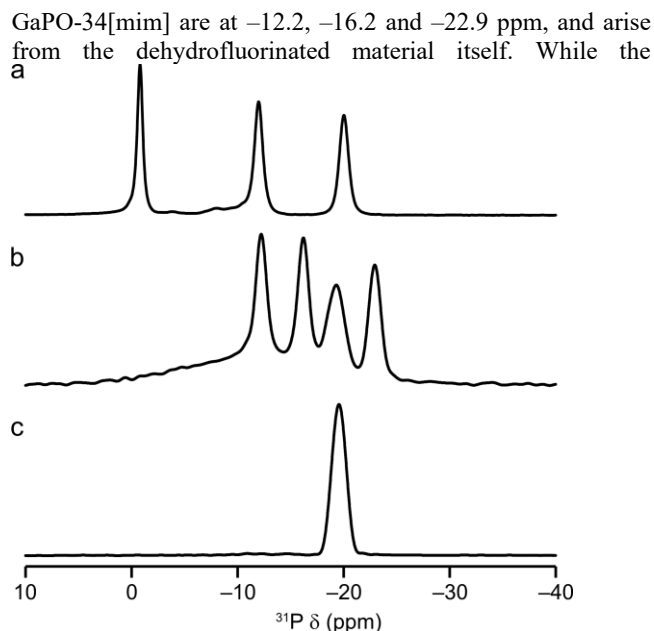
GaPO-34[mim], shown in Figure 2(b), confirm that the SDA is still present and intact in the latter, with four resonances observed at 139.2, 128.8, 124.5 and 34.8 ppm for GaPO-34[mim] (*cf.* 134.1, 124.0, 122.7 and 36.7 ppm for GaPO-34[mimHF][5]). The small differences in isotropic chemical shifts between the two materials may also be seen as evidence of deprotonation of the SDA. The ^{19}F NMR spectra of the two materials, shown in Figure 2(c), provide the clearest indication of the chemical nature of the difference between the two phases, as, while there is the expected resonance at –98.4 ppm in GaPO-34[mimHF], no ^{19}F signal is observed at all for GaPO-34[mim].

Figure 2. (a) ^{1}H (14.1 T, 55 kHz MAS), (b) ^{13}C (14.1 T, 12.5 kHz MAS) CP MAS and (c) ^{19}F (14.1 T, 55 kHz MAS) NMR spectra of GaPO-34[mimHF] (black) and GaPO-34[mim] (red). The ^{19}F NMR spectra are plotted on the same vertical intensity scale.

The spectra shown in Figure 2 therefore confirm that the first stage of the calcination of GaPO-34[mimHF] is dehydrofluorination to GaPO-34[mim].

Dehydrofluorination of GaPO-34[mimHF] to GaPO-34[mim] would be expected to result in a neutral, tetrahedral GaPO$_4$ framework, containing 1-methylimidazole within the pores. The structure of the framework was investigated further by ^{31}P NMR spectroscopy. The ^{31}P MAS NMR spectra of GaPO-34[mimHF], GaPO-34[mim] and calcined GaPO-34 are shown in Figure 3. GaPO-34[mimHF] gives rise to three resonances at –0.8, –12.0 and –20.0 ppm, assigned previously to P3, P2 and P1, respectively.[5] One broad resonance and four sharp ones are present in the ^{31}P NMR spectrum of GaPO-34[mim]. The broad resonance can be assigned to amorphous phosphate materials that are commonly observed on calcination of phosphate zeotypes. The sharp resonance at –19.3 ppm corresponds to fully-calcined GaPO-34,[5] indicating that the sample preparation temperature was too high and the sample is a mix of GaPO-34[mim] and some calcined GaPO-34 (as might be expected from the *in situ* pXRD patterns shown in Figure 1(c), where GaPO-34[mim] tends to coexist with either GaPO-34[mimHF] or the fully calcined material). In this case, it is fortuitous that a small amount of fully calcined material is present and can act as a desiccant to ensure that the GaPO-34[mim] did not take on water during the course of this study. The remaining three resonances in the ^{31}P NMR spectrum of

GaPO-34[mim] are at –12.2, –16.2 and –22.9 ppm, and arise from the dehydrofluorinated material itself. While the

Figure 3. ^{31}P (14.1 T, 25 kHz MAS) NMR spectra of (a) GaPO-34[mimHF], (b) GaPO-34[mim] and (c) calcined GaPO-34.

unchanged number of distinct resonances present indicates that the long-range structure of the framework has not changed from the as-made GaPO-34[mimHF], the differences in their positions indicate that the local structure (*i.e.*, the P-O bond lengths and P-O-Ga bond angles) must have changed significantly.[21,41] By analogy to the isostructural CHA-type aluminophosphate, AlPO-34,[42] the higher chemical shift of P3 in GaPO-34[mimHF] is a consequence of the smaller mean P-O-Ga bond angle for this site,[21,41] arising from the octahedral coordination of the two adjacent Ga1 sites. Therefore, the absence of such a high chemical shift in the ^{31}P NMR spectrum of GaPO-34[mim] is evidence of the absence of Ga-bound fluoride anions in this material.

The ^{71}Ga MAS NMR spectrum of GaPO-34[mim], shown in Figure 4, contains signals that can be identified by their chemical shifts[43] as arising from tetrahedral Ga^{IV} and five-coordinate Ga^V (δ_{iso} of *ca.* 120 and *ca.* 40 ppm, respectively), in contrast with GaPO-34[mimHF], which contains tetrahedral and octahedral Ga (δ_{iso} of 110-120 and –30 ppm, respectively,[5]
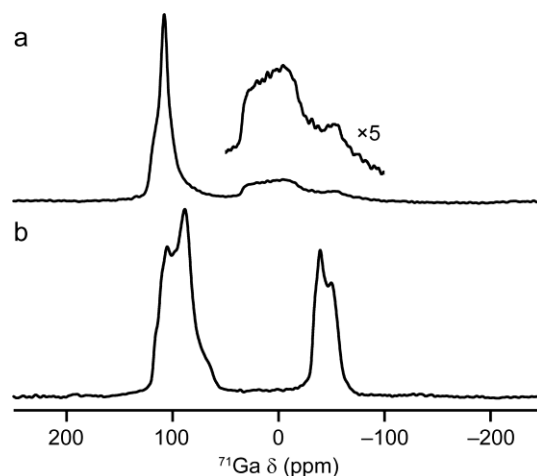

Figure 4. ^{71}Ga (20.0 T, 60 kHz MAS) spin-echo NMR spectra of

(a) GaPO-34[mim] and (b) GaPO-34[mimHF]. In (a), a vertical expansion of the Ga^V region is shown.

as seen in Figure 4(b)). The width of the Ga^V signal corresponds to a C_Q of around 10-11 MHz, typical of the lower symmetry that would be expected for a distorted trigonal bipyramidal coordination environment.[43] Although it is challenging to record truly quantitative NMR spectra for quadrupolar nuclei, especially in the presence of relatively sharp and relatively broad resonances, as is the case for GaPO-34[mim], the Ga^{IV} : Ga^V ratio obtained from the spectrum shown (acquired using pulses with short flip angles) is ~1.8 ± 0.2 : 1, which would suggest that approximately one third of the Ga atoms are five-coordinate.

In order to link the NMR spectra with the crystallographic data and in an attempt to generate a structural model for GaPO-34[mim], a series of preliminary DFT calculations on potential starting structures were carried out. It is insufficient simply to delete the water, NH proton and fluoride from the structure of GaPO-34[mimHF] since, as shown in Figure S2, this leads to a very strained coordination environment around Ga1 and, following structural optimization, neither the computed pXRD pattern (Figure S3) nor the NMR spectra were in good agreement with experiment.[44] Instead, starting from the structure of calcined GaPO-34,[45] 1-methylimidazole molecules were placed in the pores and the structure optimized. This model suggested that the Ga^V sites are formed *via* a Ga-N interaction, but the computational costs of fully optimizing this structure were very high. Therefore, a smaller model structure was generated by deleting the fluoride, NH protons and water from the unit cell of GaPO-34[mimHF], and then manually moving the 1-methylimdazole closer to the strained Ga centres. This approach led to the optimized structure shown in Figure 5a on a reasonable timescale. However, this is unlikely to be the global minimum energy structure. Figure 5b shows the local
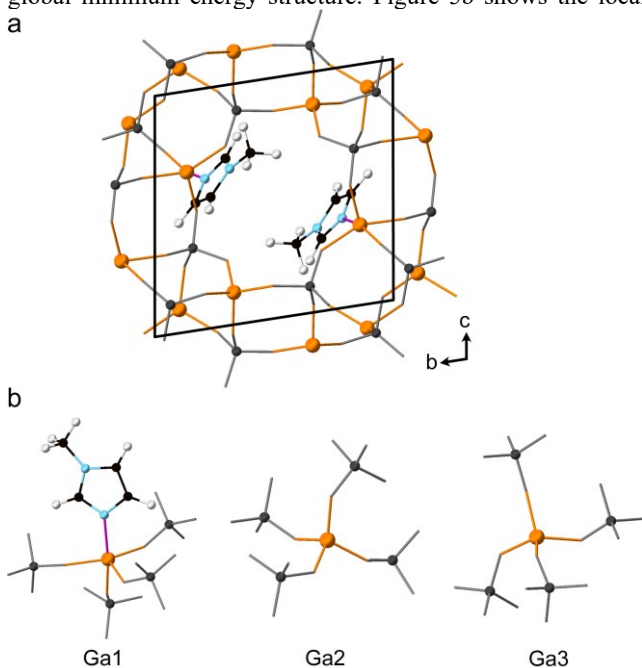
Figure 5. (a) The optimized structural model of GaPO-34[mim] obtained here, (b) local environments of the three distinct Ga atoms (in the parent $P\overline{1}$ symmetry; the model structure contains six distinct Ga sites in $P1$, but the "equivalent" pairs are very similar). Atoms are colored with H = light gray, C = black, N = light blue, P

= dark gray, Ga and Ga-O bonds = orange, and Ga-N bonds = purple.

environments for the three distinct Ga sites in the optimized structure (the structure formally has $P1$ symmetry, which would lead to six Ga and six P species, but these form very similar pairs, consistent with the parent $P\overline{1}$ symmetry of GaPO-34[mimHF]). It can be seen that Ga1 is pentacoordinate, whereas Ga2 and Ga3 remain tetrahedral, which is consistent with the approximate Ga^{IV}:Ga^V ratio observed experimentally. The pentacoordinate Ga1 site with a GaO$_4$N environment containing a direct bond to the deprotonated SDA is a motif rarely observed in gallophosphate-like materials[46,47] (and never in a fully condensed 3D GaPO$_4$ framework material, although there are a small number of fully condensed AlPOs and GaPOs that do contain similar interactions, giving rise to octahedral AlO$_4$(OH)N,[48] AlO$_4$N$_2$,[49] and GaO$_4$(OH)N[50] coordination environments). The Ga-N bond distance is 2.04 Å, which is comparable to the 2.02-2.18 Å observed in the literature.[46,47,50] The simulated pXRD pattern for this structural model of GaPO-34[mim] is in poor agreement with the experimental pattern, as shown in Figure S4. This, however, is probably to be expected, given that the temperature of the calculation is effectively 0 K and the pXRD pattern was acquired some 600 K above this. It has previously been shown that the calcined GaPO-34 framework is dynamic (leading to negative thermal expansion (NTE) behaviour).[45] While as-made zeolitic frameworks tend not to exhibit the same level of NTE owing to the pores being occupied by the SDA,[51,52] it has been demonstrated in as-made phosphate frameworks including GaPO-34A and CHA-type AlPO-34 that the SDA can be dynamic.[24,42,53] Therefore, in the partially-calcined GaPO-34[mim], it seems very likely that dynamic effects will influence the average structure at experimentally-relevant temperatures and that these will not be present in the calculated structural model.

The ^{13}C, ^{31}P and ^{71}Ga NMR spectra calculated from the optimized structural model of GaPO-34[mim] are shown overlaid with the experimental spectra in Figure 6. There is very good agreement between the calculated and experimental ^{13}C chemical shifts, confirming the deprotonated, Ga-bound chemical nature of the SDA. For ^{31}P, the calculated shifts are systematically offset by around –1 ppm from experiment: using a σ_{ref} of 291.3 ppm would give near perfect agreement for GaPO-34[mim] but would be in disagreement with the reference compound of calcined GaPO-34. There are various methods of determining σ_{ref},[25–27] including "internal referencing" (which would yield perfect agreement here), referencing to an external compound with known shift, or referencing to a series of external compounds with known shifts (which also allows the determination of any scaling factors that may be needed, here we assume a scaling factor of 1). In the present case, we have chosen not to internally reference the calculations, in order to highlight the dangers of doing so to make a structural model appear in better agreement with experiment than it may be on closer inspection (see below). For ^{71}Ga, while Ga1 is predicted to have a large C_Q (11.9 MHz) in good agreement with experiment, Ga3 is also predicted to have a high C_Q (11.3 MHz), which does not match the narrow Ga^{IV} resonance seen experimentally. The smaller predicted C_Q of 6.2 MHz for Ga2 leads to a resonance with a width in very good agreement with that observed experimentally for Ga^{IV}.

The question then arises as to why so many aspects of the local structure lead to calculated NMR parameters that agree

well with experiment, while there is a clear discrepancy for Ga3. Inspection of the local environment around Ga3 reveals
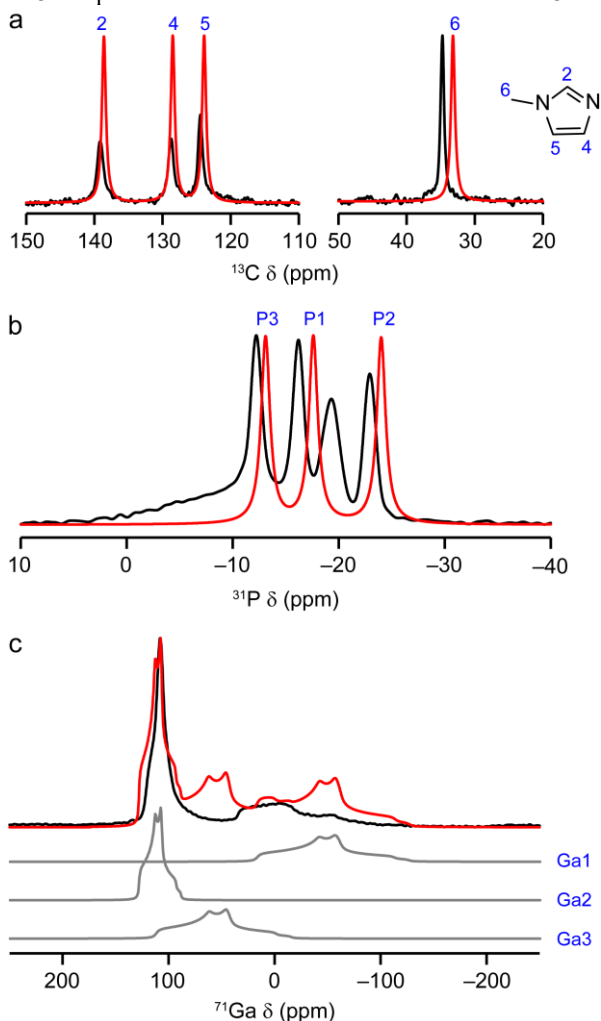
Figure 6. Experimental (black) and calculated (red) (a) ^{13}C, (b) ^{31}P and (c) ^{71}Ga NMR spectra for GaPO-34[mim]. Assignments are shown in blue. For (a) the numbering scheme is shown in the inset, and for (b) and (c) the numbering scheme is derived from GaPO-34[mimHF]. In (c) individual lineshapes for Ga1, Ga2 and Ga3 are shown in gray. In all simulated spectra, the integrated intensities of the resonances have been set to match the stoichiometry of the material, and do not reflect the non-quantitative nature of the CPMAS (for ^{13}C) or spin-echo (for ^{71}Ga) experiments.

that the Ga-O-P bond angles for this site cover a range from *ca.* 117° to *ca.* 168° (compared to a mean Ga-O-P angle of 140.0° over all sites in this structure, which is within the typical range for phosphate frameworks). One would expect such small or large bond angles to influence the ^{31}P chemical shifts of the neighboring P species.[21,41] However, since both of these Ga-O-P linkages are to different P2 within the same four-membered rings, the effects of an unusually large and unusually small Ga-O-P bond angle offset each other, and the mean P-O-Ga bond angle for P2 is 143.3° (*cf.* 139.6° for P1 and 137.3° for P3). We have previously demonstrated that, for the chemically- and structurally related AlPOs, the ^{31}P chemical shift, being an isotropic parameter, can be predicted accurately based on the mean P-O-Al angle,[21,41] whereas the ^{71}Ga C_Q, being the magnitude of an anisotropic electric field gradient, depends on the precise position of the surrounding O and P atoms. It is also

worth noting here that temperature-dependent dynamics could have a significant effect on the structure, and on some corresponding NMR parameters, at the experimental temperatures of ~300 K.[42,53] At elevated temperatures (relative to the static calculation), one would expect the P-O-Ga bonds to relax to closer to ~140° such that, while the spread of angles might decrease, the mean P-O-Ga angle for P2 would remain fairly constant. Therefore, the remarkably close agreement between the calculated and experimental ^{31}P NMR spectra in this case arise at least partially from error cancellation. We reiterate here that this serves as a valuable reminder of the importance of an accurate external reference when considering calculated chemical shifts.

Having confirmed the thermal dehydrofluorination of GaPO-34[mimHF], there remains the question of why the analogous GaPO-34[pyHF] does not undergo an equivalent transformation. It seems reasonable since the dehydrofluorinated intermediate structure contains a Ga-N interaction, that the strength of this interaction will determine the temperature range over which the neutral SDA molecules will remain in the pores of the neutral GaPO framework, before being desorbed and undergoing combustion. The pK$_a$ of pyridinium is 5.17, whereas the pK$_a$ of 1-methylimidazolium is 7.06,[54] suggesting that formation of N-Ga bonds will be significantly favoured in the presence of mim, relative to py and the pyridine will be more rapidly lost from GaPO-34[pyHF] upon dehydrofluorination (in the present case, it would appear that the two processes occur simultaneously).

The differences in SDA-framework interactions are also apparent in the DSC traces shown in Figure 1, where both materials show an endothermic event at around 380-390 °C, corresponding to breaking the Ga-F bonds. In GaPO-34[mimHF], weaker Ga-N bonds form upon dehydrofluorination, and these are then broken in a second endothermic event at around 470 °C. Conversely, in GaPO-34[pyHF], once the Ga-F bonds are broken, no Ga-N bonds form and the SDA is lost alongside the HF in a single endothermic event.

Conclusions

Using a combination of thermogravimetry, *in situ* pXRD and multinuclear solid-state NMR spectroscopy, it was demonstrated that the calcination of GaPO-34[mimHF] unexpectedly occurs *via* an intermediate dehydrofluorination step to give GaPO-34[mim], in which neutral 1-methylimidazole molecules remain intact in the pores. A structural model was generated computationally and, following optimization, the computed ^{13}C and ^{31}P NMR parameters are in good agreement with experiment, while the computed pXRD pattern and ^{71}Ga NMR parameters display poorer agreement, suggesting the model is a good representation of the local structure but not necessarily of the longer-range structure at higher temperature.

The optimized structure contains an unusual pentacoordinate Ga species, owing to the formation of a Ga···N Lewis adduct between the neutral imidazole SDA and the framework, and the calculated ^{71}Ga NMR parameters for this site match reasonably well with experiment. However, the structural model also contains surprisingly acute (~118°) and obtuse (~168°) Ga-O-P linkages, which would be unlikely to remain in that geometry at room temperature. These results show that, even if perfect agreement with experiment cannot be achieved (especially

between the pXRD patterns obtained experimentally at relatively high temperature and a structural model optimized at effectively 0 K), DFT calculations can be of great value to explore possible structural models and exemplify the types of local environment that may be present in an unknown structure.

However, these results also demonstrate that there remains a need for a more rigorous approach to understanding the effects of dynamics in phosphates (and other zeolitic frameworks), in order to be able to combine more effectively high-temperature *in situ* pXRD, room-temperature NMR spectroscopy and "0 K" DFT structures. In recent years, various unbiased computational methods for generating possible structural models have emerged[55-58] along with novel approaches for modelling the effects of dynamic processes on spectroscopic parameters.[59-62] As illustrated by the challenges described in this work, it seems likely that these computational methods will gain increasing prominence in the field of NMR crystallography. However, it remains to be seen how effective these methods will be for mixed organic/inorganic framework materials, rather than the dense phases and molecular crystals to which they are typically applied at present.

The structure of GaPO-34[mim] provides some clue as to why GaPO-34[mimHF] undergoes dehydrofluorination prior to calcination, whereas GaPO-34[pyHF] does not: the higher pK_a of 1-methylimidazolium relative to pyridine suggests that the Ga-N interaction would be weaker for py than mim, such that the pyridine will not remain in the pores of the GaPO once the electrostatic attraction to the framework is lost upon dehydrofluorination. This observation suggests that it may be possible to design a form of GaPO-34 containing an SDA with even higher pKa (*e.g.*, 1,4-dimethylimidazolium), such that the dehydrofluorination and SDA loss events are separated by a greater temperature window, allowing the material to act as a clean solid source of HF.

ASSOCIATED CONTENT

Supporting Information

Additional discussion of the TGA data, ^{71}Ga NMR spectrum of GaPO-34[mim], further computational details and complete references 26 and 49 are given in the Supporting Information. The Supporting Information is available free of charge on the ACS Publications website.

AUTHOR INFORMATION

Corresponding Author

*dmd7@st-andrews.ac.uk (D. M. D.)
*sema@st-andrews.ac.uk (S. E. A.)

Notes

The authors declare no competing financial interest.

REFERENCES

1. Wright, P. A. *Microporous Framework Solids*, **2008**, Royal Society of Chemistry, Cambridge, UK.
2. Wilson, S. T.; Lok, B. M.; Messina, C. A.; Cannan, T. R.; Flanigen, E. M. Aluminophosphate Molecular Sieves: A new Class of Microporous Crystalline Inorganic Solids. *J. Am. Chem. Soc.* **1982**, *104*, 1146–1147.
3. Girard, S.; Gale, J. D.; Mellot-Draznieks, C.; Férey, G. Framework Stability of Nanoporous Inorganic Structures upon Template Extraction and Calcination: A Theoretical Study of Gallophosphate Polymorphs. *J. Am. Chem. Soc.* **2002**, *124*, 1040–1051.
4. Schott-Darie, C.; Kessler, H.; Soulard, M.; Gramlich, V.; Benazzi, E. Diversity of the System Ga$_2$O$_3$-P$_2$O$_5$-H$_2$O-HF in the Presence of Organic Species. *Stud. Surf. Sci. Catal.*, **1994**, *84*, 101–108.
5. Amri, M.; Ashbrook, S. E.; Dawson, D. M.; Griffin, J. M.; Walton, R. I.; Wimperis, S. A Multinuclear Solid-State NMR Study of Templated and Calcined Chabazite-Type GaPO-34. *J. Phys. Chem. C* **2012**, *116*, 15048–15057.
6. Harris, R. K., Wasylishen, R. E., Duer, M. J., Eds. *NMR Crystallography*; John Wiley & Sons: Chichester, U.K., 2009.
7. Taulelle, F.; Bouchevreau, B.; Martineau, C. NMR Crystallography Driven Structure Determination: Nanoporous Materials. *CrystEngComm* **2013**, *15*, 8613–8622.
8. Florian, P.; Massiot, D. Beyond Periodicity: Probing Disorder in Crystalline Materials by Solid-State Nuclear Magnetic Resonance Spectroscopy. *CrystEngComm* **2013**, *15*, 8623–8626.
9. Taulelle, F. NMR Crystallography: Crystallochemical Formula and Space Group Selection. *Solid State Sci.* **2004**, *6*, 1053–1057.
10. Martineau, C.; Cadiau, A.; Bouchevreau, B.; Senker, J.; Taulelle, F.; Adil, K. SMARTER Crystallography of the Fluorinated Inorganic−Organic Compound Zn$_3$Al$_2$F$_{12}$·[HAmTAZ]$_6$. *Dalton Trans.* **2012**, *41*, 6232–6241.
11. Bryce, D. L. NMR Crystallography: Structure and Properties of Materials from Solid-State Nuclear Magnetic Resonance Observables. *IUCrJ* **2017**, *4*, 350–359.
12. Martineau-Corcos, C. NMR Crystallography: A Tool for the Characterization of Microporous Hybrid Solids. *Curr. Opin. Colloid Interface Sci.* **2018**, *33*, 35–43.
13. Brouwer, D. H. NMR Crystallography of Zeolites: Refinement of an NMR-Solved Crystal Structure Using ab Initio Calculations of ^{29}Si Chemical Shift Tensors. *J. Am. Chem. Soc.* **2008**, *130*, 6306–6307.
14. Brouwer, D. H. Structure Solution of Network Materials by Solid-State NMR without Knowledge of the Crystallographic Space Group. *Solid State Nucl. Magn. Reson.* **2013**, *51*, 37–45.
15. Brouwer, D. H.; Darton, R. J.; Morris, R. E.; Levitt, M. H. A Solid-State NMR Method for Solution of Zeolite Crystal Structures. *J. Am. Chem. Soc.* **2005**, *127*, 10365–10370.
16. Brouwer, D. H.; Moudrakovski, I. L.; Darton, R. J.; Morris, R. E. Comparing Quantum-Chemical Calculation Methods for Structural Investigation of Zeolite Crystal Structures by Solid-State NMR Spectroscopy. *Magn. Reson. Chem.* **2010**, *48*, S113–S121.
17. Brouwer, D. H.; Langendoen, K. P. A Graph Theory Approach to Structure Solution of Network Materials from Two-Dimensional Solid-State NMR Data. *CrystEngComm* **2013**, *15*, 8748–8762.
18. Brouwer, D. H.; Van Huizen, J. NMR Crystallography of Zeolites: How Far Can We Go without Diffraction Data? *Magn. Reson. Chem.* **2019**, *57*, 167–175.
19. Martineau, C.; Mellot-Draznieks, C.; Taulelle, F. NMR Crystallography of AlPO4-CJ2: from the Topological Network to the Local (OH)/F Distribution. *Phys. Chem. Chem. Phys.* **2011**, *13*, 18078–18087.

20. Martineau, C.; Bouchevreau, B.; Tian, Z.; Lohmeier, S.-J.; Behrens, P.; Taulelle, F. Beyond the Limits of X-ray Powder Diffraction: Description of the Nonperiodic Subnetworks in Aluminophosphate-Cloverite by NMR Crystallography. *Chem. Mater.* **2011**, *23*, 4799–4809.

21. Dawson, D. M.; Seymour, V. R.; Ashbrook, S. E. Effects of Extraframework Species on the Structure-Based Prediction of ^{31}P Isotropic Chemical Shifts of Aluminophosphates. *J. Phys. Chem. C* **2017**, *121*, 28065–28076.

22. Bouchevreau, B.; Martineau, C.; Mellot-Draznieks, C.; Tuel, A.; Suchomel, M. R.; Trébosc, J.; Lafon, O.; Amoureux, J.-P.; Taulelle, F. An NMR-Driven Crystallography Strategy to Overcome the Computability Limit of Powder Structure Determination: A Layered Aluminophosphate Case. *Chem. - Eur. J.* **2013**, *19*, 5009–5013.

23. Seymour, V. R.; Eschenroeder, E. C. V.; Castro, M.; Wright, P. A.; Ashbrook, S. E. Application of NMR Crystallography to the Determination of the Mechanism of Charge-Balancing in Organocation- Templated AlPO STA-2. *CrystEngComm* **2013**, *15*, 8668–8679.

24. Ashbrook, S. E.; Dawson, D. M.; Gan, Z.; Hooper, J. E.; Hung, I.; Macfarlane, L. E.; McKay, D.; McLeod, L. K.; Walton, R. I. Application of NMR Crystallography to Highly Disordered Templated Materials: Extensive Local Structural Disorder in the Gallophosphate GaPO-34A. *Inorg. Chem.* **2020** *59*, 11616–11626.

25. Charpentier, T. The PAW/GIPAW Approach for Computing NMR Parameters: A new Dimension Added to NMR Study of Solids. *Solid State Nucl. Magn. Reson.* **2011**, *40*, 1–20.

26. Bonhomme, C.; Gervais, C.; Babonneau, F.; Coelho, C.; Pourpoint, F.; Azaïs, T.; Ashbrook, S. E.; Griffin, J. M.; Yates, J. R.; Mauri, F. *et al.* First-Principles Calculation of NMR Parameters Using the Gauge Including Projector Augmented Wave Method: A Chemist's Point of View. *Chem. Rev.* **2012**, *112*, 5733–5779.

27. Ashbrook, S. E.; McKay, D. Combining Solid-State NMR Spectroscopy with First-Principles Calculations – a Guide to NMR Crystallography. *Chem. Commun.* **2016**, *52*, 7186–7204.

28. Oliver, S.; Kuperman, A.; Lough, A.; Ozin, G. A. Synthesis and Characterization of a Fluorinated Anionic Aluminophosphate Framework UT-6, and its High-Temperature Dehydrofluorination to AlPO$_4$-CHA. *J. Mater. Chem.* **1997**, *7*, 807–812.

29. Wang, D.; Xu, S.; Yang, M.; Chu, Y.; Tian, P.; Liu, Z. Microporous Aluminophosphate ULM-6: Synthesis, NMR Assignment, and Its Transformation to AlPO$_4$-14 Molecular Sieve. *J. Phys. Chem. C*, **2016**, *120*, 11854–11863.

30. Broom, L. K.; Clarkson, G. J.; Guillou, N.; Hooper, J. E.; Dawson, D. M.; Tang, C. C.; Ashbrook, S. E.; Walton, R. I. A Gel Aging Effect in the Synthesis of Open-Framework Gallium Phosphates: Structure Solution and Solid-State NMR of a Large-Pore, Open-Framework Material. *Dalton Trans.* **2017**, *46*, 16895–16904.

31. Cory, D. G.; Ritchey, W. M. Suppression of Signals from the Probe in Bloch Decay Spectra. *J. Magn. Reson.* **1988**, *80*, 128–132.

32. Clark, S. J.; Segall, M. D.; Pickard, C. J.; Hasnip, P. J.; Probert, M. J.; Refson, K.; Payne, M. C. First Principles Methods using CASTEP. *Z. Kristallogr.* **2005**, *220*, 567–570.

33. Pickard, C. J.; Mauri, F. All-Electron Magnetic Response with Pseudopotentials: NMR Chemical Shifts. *Phys. Rev. B* **2001**, *63*, 245101.

34. Yates, J. R.; Pickard, C. J.; Mauri, F. Calculation of NMR Chemical Shifts for Extended Systems using Ultrasoft Pseudopotentials. *Phys. Rev. B* **2007**, *76*, 024401.

35. Yates, J. R.; Pickard, C. J.; Payne, M. C.; Mauri, F. Relativistic Nuclear Magnetic Resonance Chemical Shifts of Heavy Nuclei with Pseudopotentials and the Zeroth-Order Regular Approximation. *J. Chem. Phys.* **2003**, *118*, 5746–5753.

36. Cook, D. S.; Hooper, J. E.; Dawson, D. M.; Ashbrook, S. E.; Fisher, J. M.; Thompsett, D.; Walton, R. I. Synthesis and Polymorphism of Mixed Aluminum-Gallium Oxides. *Inorg. Chem.* **2020**, *59*, 3805–3816.

37. Tkatchenko, A.; Scheffler, M. Accurate Molecular van der Waals Interactions from Ground-State Electron Density and Free-Atom Reference Data. *Phys. Rev. Lett.* **2009**, *102*, 073005.

38. McNellis, E. R.; Meyer, J.; Reuter, K. Azobenzene at Coinage

Metal Surfaces: Role of Dispersive van der Waals Interactions. *Phys. Rev. B* **2009**, *80*, 205414.

39. The experimental structure of as-made GaPO-34 contains a disordered water molecule, which distorts the framework geometry. When this is removed and the structure is optimized again, the P-O-Ga bond angles change and the computed ^{31}P and ^{71}Ga magnetic shieldings require significant scaling to be made to (incorrectly) match experiment (σ_{ref} = 214.9 ppm, m = 0.75 for ^{31}P, σ_{ref} = 1703 ppm, m = 0.98 for ^{71}Ga). However, the 1-methyimidazolium SDA is not affected significantly by the hydration state of the material and the calculated ^{13}C shifts are in good agreement with experiment.

40. Pyykko, P. Year-2017 Nuclear Quadrupole Moments. *Mol. Phys.* **2018**, *116*, 1328–1338.

41. Dawson, D. M.; Ashbrook, S. E. Investigating Relationships between the Crystal Structure and ^{31}P Isotropic Chemical Shifts in Calcined Aluminophosphates. *J. Phys. Chem. C* **2014**, *118*, 23285–23296.

42. Dawson, D. M.; Griffin, J. M.; Seymour, V. R.; Wheatley, P. S.; Amri, M.; Kurkiewicz, T.; Guillou, N.; Wimperis, S.; Walton, R. I.; Ashbrook, S. E. A Multinuclear NMR Study of Six Forms of AlPO-34: Structure and Motional Broadening. *J. Phys. Chem. C* **2017**, *121*, 1781–1793.

43. Massiot, D.; Vosegaard, T.; Magneron, N.; Trumeau, D.; Montouillout, V.; Berthet, P.; Loiseau, T.; Bujoli, B. ^{71}Ga NMR of Reference Ga$_{IV}$, Ga$_V$, and Ga$_{VI}$ Compounds by MAS and QPASS, Extension of Gallium/Aluminum NMR Parameter Correlation. *Solid State Nucl. Mag. Reson.*, **1999**, *15*, 159–169.

44. Dawson, D. M. Combined Theoretical and Experimental Investigations of Porous Crystalline Materials. *PhD. Thesis*, University of St Andrews, UK, **2014**.

45. Amri, M.; Walton, R. I. Negative Thermal Expansion in the Aluminum and Gallium Phosphate Zeotypes with CHA and AEI Structure Types. *Chem. Mater.* **2009**, *21*, 3380–3390.

46. Chen, C.-Y.; Chu, P. P.; Lii, K.-H. Synthesis, Crystal Structure and ^{71}Ga MAS NMR Spectroscopy of a Novel Gallium Phosphatooxalate: [Ga$_5$(OH)$_2$(C$_{10}$H$_9$N$_2$)(C$_2$O$_4$)(PO$_4$)$_4$]·2H$_2$O. *Chem. Commun.*, **1999**, 1473–1474.

47. Chen, C.-Y.; Lii, K. H.; Jacobson, A. J. Synthesis and Characterization of Organic–Inorganic Hybrid Compounds with a Pillared Layer Structure: Ga$_2$(4,4′-bpy)(XO$_4$)$_2$ (X=P, As). *J. Solid State Chem.*, **2003**, *172*, 252–256.

48. Jordá, J. L.; McCusker, L. B.; Baerlocher, C.; Morais, C. M.; Rocha, J.; Fernandez, C.; Borges, C.; Lourenço, J. P.; Ribeiro, M. F.; Gabelica, Z. Structure Analysis of the Novel Microporous Aluminophosphate IST-1 Using Synchrotron Powder Diffraction Data and HETCOR MAS NMR. *Micropor. Mesopor. Mater.* **2003**, *65*, 43–57.

49. Watts, A. E.; Lozinska, M. M.; Slawin, A. M. Z.; Mayoral, A.; Dawson, D. M.; Ashbrook, S. E.; Bode, B. E.; Dugulan, A. I.; Shannon, M. D.; Cox, P. A. *et al.* Site-Specific Iron Substitution in STA-28, a Large Pore Aluminophosphate Zeotype Prepared by Using 1,10-Phenanthrolines as Framework-Bound Templates. *Angew. Chem. Int. Ed.*, **2020**, *59*, 15186–15190.

50. Brouca-Cabarrecq, C.; Mosset, A. New Potential Open-Framework Materials in Gallophosphate Systems. Preparation and Crystal Structure of [NH$_3$(CH$_2$)$_3$NH$_3$]Ga$_3$(PO$_4$)$_3$(OH)$_2$·H$_2$O and [NH$_2$(CH$_2$)$_3$NH$_2$]Ga$_3$(PO$_4$)$_3$(H$_2$O). *J. Mater. Chem.*, **2000**, *10*, 445–450.

51. Lightfoot, P.; Woodcock, D. A.; Maple, M. J.; Villaescusa, L. A.; Wright, P. A. The Widespread Occurrence of Negative Thermal Expansion in Zeolites. *J. Mater. Chem.*, **2001**, *11*, 212–216.

52. Sneddon, S.; Dawson, D. M.; Pickard, C. J.; Ashbrook, S. E. Calculating NMR Parameters in Aluminophosphates: Evaluation of Dispersion Correction Schemes. *Phys. Chem. Chem. Phys.* **2014**, *16*, 2660–2673.

53. Antonijevic, S.; Ashbrook, S. E.; Biedasek, S.; Walton, R. I.; Wimperis, S.; Yang, H. Dynamics on the Microsecond Timescale in Microporous Aluminophosphate AlPO-14 as Evidenced by ^{27}Al MQMAS and STMAS NMR Spectroscopy. *J. Am. Chem. Soc.*, **2006**, *128*, 8054–8062.

54. *Lange's Handbook of Chemistry*, 15th ed., Ed. Dean, J. A. **1998**,

McGraw-Hill, New York, NY.

55. Pickard, C. J.; Needs, R. J. *Ab Initio* Random Structure Searching. *J. Phys.: Condens. Matter* **2011**, *23*, 053201.

56. Charpentier, T.; Menziani, M. C.; Pedone, A. Computational Simulations of Solid State NMR Spectra: A New Era in Structure Determination of Oxide Glasses. *RSC Adv.* **2013**, *3*, 10550–10578.

57. Day, G. M. Current Approaches to Predicting Molecular Organic Crystal Structures. *Crystallogr. Rev.* **2011**, *17*, 3–52.

58. Grau-Crespo, R.; Hamad, S.; Catlow, C. R. A.; de Leeuw, N. H. Symmetry-Adapted Configurational Modelling of Fractional Site Occupancy in Solids. *J. Phys.: Condens. Matter* **2007**, *19*, 256201.

59. Monserrat, B.; Needs, R. J.; Pickard, C. J. Temperature Effects in First-Principles Solid State Calculations of the Chemical Shielding Tensor Made Simple. *J. Chem. Phys.* **2014**, *141*, 134113.

60. Dračínský, M.; Bouř, P.; Hodgkinson, P. Temperature Dependence of NMR Parameters Calculated from Path Integral Molecular Dynamics Simulations. *J. Chem. Theory Comput.* **2016**, *12*, 3, 968–973.

61. Nemausat, R.; Cabaret, D.; Gervais, C.; Brouder, C.; Trcera, N.; Bordage, A.; Errea, I.; Mauri, F. Phonon Effects on X-ray Absorption and Nuclear Magnetic Resonance Spectroscopies. *Phys. Rev. B.*, **2015**, *92*, 144310.

62. Nemausat, R.; Gervais, C.; Brouder, C.; Trcera, N.; Bordage, A.; Coelho-Diogo, C.; Florian, P.; Rakhmatullin, A.; Errea, I.; Paulatto, L. *et al.* Temperature Dependence of X-ray Absorption and Nuclear Magnetic Resonance Spectra: Probing Quantum Vibrations of Light Elements in Oxides. *Phys. Chem. Chem. Phys.*, **2017**, *19*, 6246–6256.

63. Dawson, D. M.; Macfarlane, L. E.; Amri, M.; Walton, R. I.; Ashbrook, S. E. The Thermal Dehydrofluorination of GaPO-34 Revealed by NMR Crystallography. Dataset. https://doi.org/10.17630/5dedf5bf-1cb4-41b0-9f2c-be5341b61b6c.

TOC entry

GaPO-34

as-made   −HF   calcined

GaO_4F_2 GaO_4N GaO_4